Molecular Therapy
Methods & Clinical Development
Original Article

Systemic γ-sarcoglycan AAV gene transfer results in dose-dependent correction of muscle deficits in the LGMD 2C/R5 mouse model

Young-Eun Seo,[1] Stephen H. Baine,[1] Amber N. Kempton,[1] Oliver C. Rogers,[1] Sarah Lewis,[1] Kaitlin Adegboye,[1] Alex Haile,[1] Danielle A. Griffin,[1] Ellyn L. Peterson,[1] Eric R. Pozsgai,[1] Rachael A. Potter,[1] and Louise R. Rodino-Klapac[1]

[1]Research & Development, Gene Therapy Research, Sarepta Therapeutics, Inc., Cambridge, MA, USA

Limb-girdle muscular dystrophy (LGMD) type 2C/R5 results from mutations in the γ-sarcoglycan (*SGCG*) gene and is characterized by muscle weakness and progressive wasting. Loss of functional γ-sarcoglycan protein in the dystrophin-associated protein complex destabilizes the sarcolemma, leading to eventual myofiber death. The *SGCG* knockout mouse (*SGCG*$^{-/-}$) has clinical-pathological features that replicate the human disease, making it an ideal model for translational studies. We designed a self-complementary rAAVrh74 vector containing a codon-optimized human *SGCG* transgene driven by the muscle-specific MHCK7 promoter (SRP-9005) to investigate adeno-associated virus (AAV)-mediated *SGCG* gene transfer in *SGCG*$^{-/-}$ mice as proof of principle for LGMD 2C/R5. Gene transfer therapy resulted in widespread transgene expression in skeletal muscle and heart, improvements in muscle histopathology characterized by decreased central nuclei and fibrosis, and normalized fiber size. Histopathologic improvements were accompanied by functional improvements, including increased ambulation and force production and resistance to injury of the tibialis anterior and diaphragm muscles. This study demonstrates successful systemic delivery of the *hSGCG* transgene in *SGCG*$^{-/-}$ mice, with functional protein expression, reconstitution of the sarcoglycan complex, and corresponding physiological and functional improvements, which will help establish a minimal effective dose for translation of SRP-9005 gene transfer therapy in patients with LGMD 2C/R5.

INTRODUCTION

Limb-girdle muscular dystrophy (LGMD) refers to a genetically diverse group of muscular dystrophies with many subtypes that are each caused by a unique mutation and compilation of symptoms.[1,2] Sarcoglycanopathies comprise four major LGMD subtypes, namely 2C/R5, 2D/R3, 2E/R4, and 2F/R6, each of which is caused by mutations in the gene that encodes an integral sarcoglycan protein subunit within the sarcoglycan complex (γ-sarcoglycan [*SGCG* gene], α-sarcoglycan [*SGCA* gene], β-sarcoglycan [*SGCB* gene], and δ-sarcoglycan [*SGCD* gene], respectively).[1,2] Because sarcoglycans play a vital role in preventing muscle damage during muscle contraction, the clinical hallmark of LGMD is weakening and atrophy of proximal muscles, specifically in the limb-girdle region, with some variability in the age of onset, severity, prognosis, and disease progression among LGMD subtypes.[1,2]

LGMD subtype 2C/R5 (LGMD 2C/R5), often referred to as γ-sarcoglycanopathy, is an autosomal recessive disease that causes loss of functional protein with impairment of the sarcoglycan complex and other structural components of the dystrophin-associated protein complex (DAPC).[1,3,4] Notably, loss of the γ-sarcoglycan protein leads to a progressive muscular dystrophy with deteriorating muscle function, with onset from 1 to 15 years of age.[5] It presents as progressive muscle weakening starting in the girdle muscles before extending to lower and upper extremities and can also present in the diaphragm and heart, resulting in respiratory and cardiac failure in some patients.[6] Symptoms include calf hypertrophy, scapular winging, macroglossia, lumbar hyperlordosis, difficulty walking/running, weakness in proximal muscles caused by fat replacement and fibrosis, elevated creatine kinase (CK), scoliosis, and joint contractures.[5,7] The debilitating disease often leads to wheelchair dependency around adolescence and premature death due to cardiac or respiratory failure.[5,8] Currently there are no approved disease-modifying therapies for LGMD 2C/R5.[9]

The *SGCG*-deficient (*SGCG*$^{-/-}$) mouse model of LGMD 2C/R5 lacks the *SGCG* gene and exhibits complete loss of the γ-sarcoglycan protein. Its phenotype accurately recapitulates the clinical-pathological features seen in LGMD 2C/R5 patients. *SGCG*$^{-/-}$ mice develop a form of muscular dystrophy and cardiomyopathy, with disease manifestations including necrosis, fatty infiltration, central nucleation, fibrosis, atrophy, and hypertrophy. Histologically, muscle tissue from untreated *SGCG*$^{-/-}$ mice exhibits significant cycles of degeneration and regeneration, indicated by centralized nuclei, increased

Received 3 January 2022; accepted 13 January 2023;
https://doi.org/10.1016/j.omtm.2023.01.004.

Correspondence: Louise Rodino-Klapac, Research & Development, Sarepta Therapeutics Inc., 4201 Easton Commons, Columbus, OH 43219, USA.
E-mail: lrodinoklapac@sarepta.com

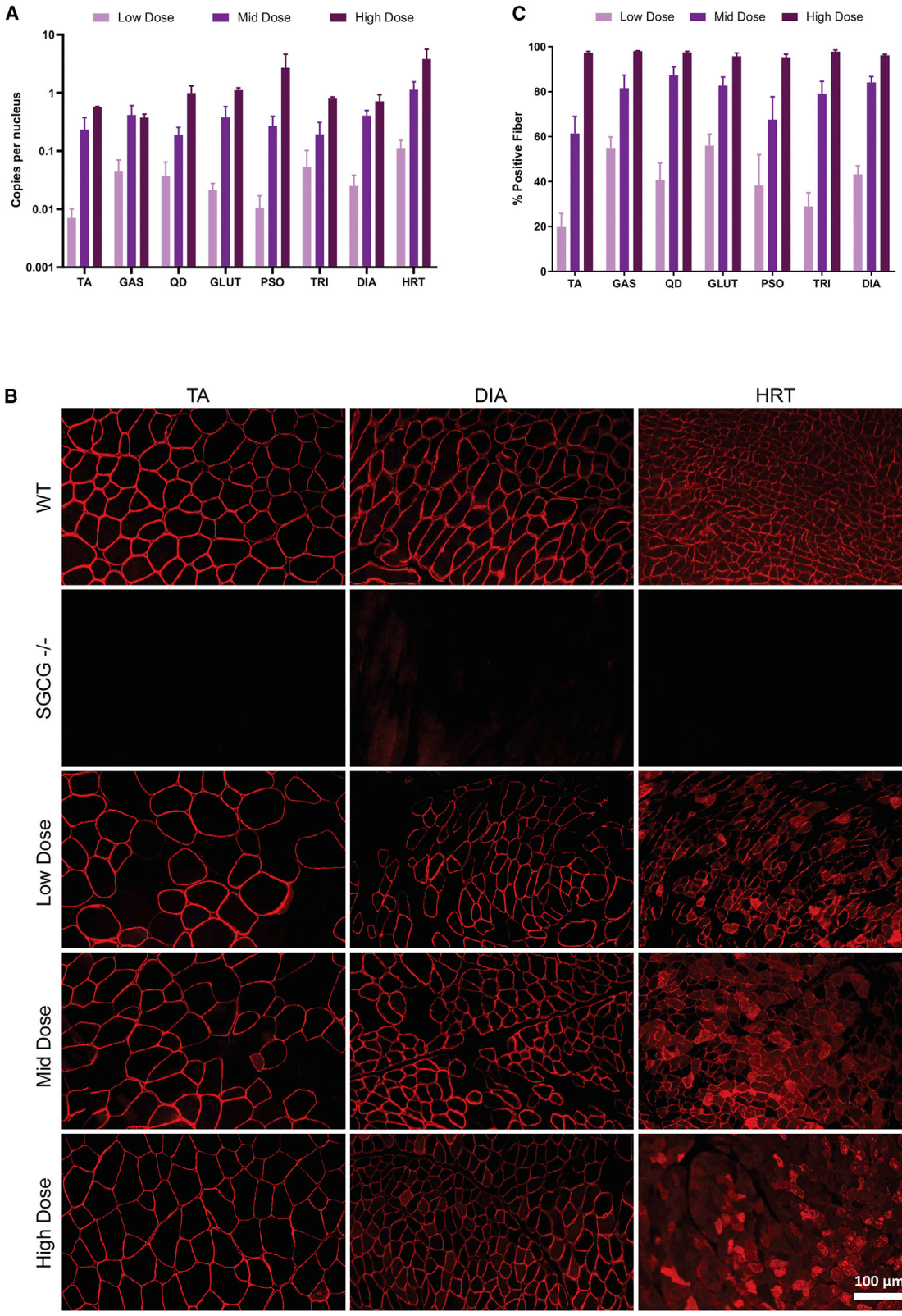

(legend on next page)

fiber size distribution, and high levels of creatinine kinase activity. Additionally, owing to the deterioration of skeletal, diaphragm, and cardiac muscle functions, untreated *SGCG*$^{-/-}$ mice experience increased fatigue, reduced diaphragm force outputs, and decreased overall activity,[10,11] making the *SGCG*$^{-/-}$ mice an ideal model to study and assess the effects of disease-modifying therapies.

Gene transfer therapy has emerged as a promising treatment for monogenic diseases such as LGMD, including LGMD 2C/R5.[4,5] Adeno-associated virus (AAV)-mediated gene transfer therapy has shown potential to treat sarcoglycanopathies and other neuromuscular diseases, including γ-sarcoglycanopathy.[12–16] Intramuscular administration of AAV-γ-sarcoglycan gene therapy rescued the dystrophic phenotype in *SGCG*$^{-/-}$ mice[17] and restore γ-sarcoglycan expression in a phase I trial that included LGMD 2C/R5 patients.[18] Systemic delivery of another AAV-γ-sarcoglycan gene therapy in *SGCG*$^{-/-}$ mice highlighted the requirement for a threshold level of transgene expression necessary for myofiber stabilization.[19]

To restore functional γ-sarcoglycan protein to muscles, we designed a self-complementary recombinant AAVrh74.MHCK7.hSGCG construct (SRP-9005). The recombinant AAVrh74 vector (rAAVrh74) has been shown in mice, non-human primates, and humans to be safe and highly efficient in transducing muscle across the vascular barrier, displaying robust muscle tissue tropism.[20–23] Furthermore, patients with muscular dystrophy have relatively low levels of pre-existing immunity.[20,23,24] rAAVrh74 has been used in several studies to successfully deliver transgenes, including GALGT2,[22] dysferlin,[25] β-sarcoglycan,[12,26] α-sarcoglycan,[27] and micro-dystrophin.[13] The MHCK7 promoter selectively regulates and drives transgene expression in skeletal and cardiac muscle and includes an α-myosin heavy chain enhancer to drive strong expression in cardiac muscle.[28] The hSGCG transgene carries full-length *SGCG* codon-optimized cDNA. One of the rate-limiting steps of AAV transduction and subsequent transgene expression is the conversion of the single-stranded vector genome into a double-stranded genome through the synthesis of a cDNA strand.[29,30] Because of the small size of the SGCG transgene, we are able to bypass this critical rate-limiting step by using a self-complementary vector cassette that packages a double-stranded transgene through complementary base-pairing and a mutated hairpin inverted terminal repeat (ITR).[31]

In this dose-escalation study, we examine the safety and efficacy of systemic gene transfer of SRP-9005 in *SGCG*$^{-/-}$ mice. We demonstrate successful systemic delivery of SRP-9005 by widespread vector transduction, robust transgene expression in all skeletal muscles, biological restoration of γ-sarcoglycan protein and the full sarcoglycan complex at the sarcolemma, improvement in muscle physiopathology, functional restoration of muscle strength, resistance to contraction-induced injury, and improvements in ambulation.

RESULTS

A single intravenous injection of SRP-9005 was given via lateral tail vein to 4-week-old *SGCG*$^{-/-}$ mice at one of three doses, based on linear plasmid standard for qPCR: low (4.63×10^{12} vector genomes [vg]/kg), mid (1.85×10^{13} vg/kg), or high (7.41×10^{13} vg/kg). Saline was administered to 4-week-old *SGCG*$^{-/-}$ mice as a negative control and to 4-week-old wild-type (WT) mice as a positive control. At 12 weeks post treatment, tissue analyses were performed on all skeletal muscles, diaphragm, heart, and internal organs to assess hSGCG transgene transduction and expression, γ-sarcoglycan protein production, rescue of the sarcoglycan complex, and changes in muscle physiopathology. Muscle function was also assessed.

Biodistribution

A single systemic injection of SRP-9005 resulted in successful delivery of hSGCG transgene by rAAVrh74 vector to targeted muscle tissue as shown by biodistribution of vector genome copies per nucleus, measured by qPCR (Figure 1A). Vector genomes were present in every tissue tested with highest values in muscle and clearance organs, including high copy numbers in the diaphragm and heart. Vector genome copies per nucleus increased with higher doses, indicating that SRP-9005 transduction was dose dependent. At the highest dose, the majority of tested tissues showed at least one vector genome per nucleus.

Expression

Transgene expression was assessed by immunofluorescence and western blot analyses. SRP-9005 delivery to *SGCG*$^{-/-}$ mice resulted in robust protein production in skeletal muscle, diaphragm, and heart (Figure 1B). Quantitative analysis of γ-sarcoglycan percent-positive fibers (PPFs) demonstrated a dose-dependent increase in γ-sarcoglycan expression in all skeletal muscles examined, including the tibialis anterior, gastrocnemius, quadriceps, gluteus, psoas, triceps, and diaphragm (Figure 1C). Mean PPFs ranged from 20% to 56% after low-dose treatment, 61%–87% with mid-dose treatment, and 95%–98% after the highest dose of SRP-9005. Because of the unique morphology of heart tissue and cytoplasmic staining at the highest dose, immunofluorescence was limited to qualitative analysis in the heart. Western blot confirmed dose-dependent γ-sarcoglycan protein production across non-cardiac muscle tissues (mean percentage of WT: low dose, 3%–41%; mid dose, 20%–99%; high dose, 41%–217%; Figures 2A and 2B) and in the heart, with expression

Figure 1. Biodistribution and expression

(A) Biodistribution of vector genome copies across muscle groups (TA, GAS, QD, GLUT, PSO, TRI, DIA, HRT), quantified by qPCR for mice systemically treated with low dose (8.94×10^{10} vg total dose; 4.63×10^{12} vg/kg), mid dose (3.63×10^{11} vg total dose; 1.85×10^{13} vg/kg), or high dose (1.26×10^{12} vg total dose; 7.41×10^{13} vg/kg) of SRP-9005 (n = 6/group). Data represent the mean ± SEM. (B) Representative immunofluorescence images of γ-sarcoglycan stain of tibialis anterior, diaphragm, and heart muscles from mice systemically treated with low, mid, or high dose of SRP-9005 (n = 6/muscle group). Scale bar, 100 μm. (C) Positive fiber expression for low, mid, and high dose of SRP-9005 (n = 6/muscle group). DIA, diaphragm; GAS, gastrocnemius; GLUT, gluteus; HRT, heart; PSO, psoas major; QD, quadriceps; *SGCG*$^{-/-}$, γ-sarcoglycan gene deficient; TA, tibialis anterior; TRI, triceps; WT, wild type.

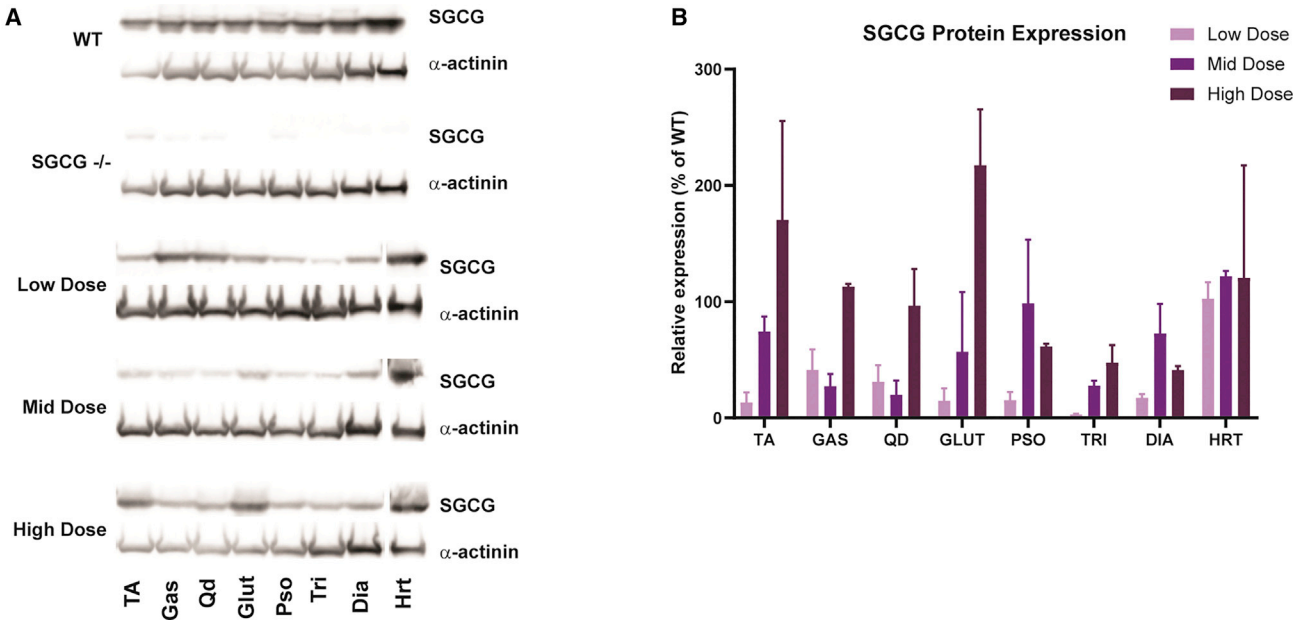

Figure 2. Expression and quantification by western blot

(A) Representative western blots of muscles (TA, GAS, QD, GLUT, PSO, TRI, DIA, HRT) and (B) densitometry quantification from *SGCG*$^{-/-}$ mice treated systemically with low dose (8.94×10^{10} vg total dose; 4.63×10^{12} vg/kg), mid dose (3.63×10^{11} vg total dose; 1.85×10^{13} vg/kg), or high dose (1.26×10^{12} vg total dose; 7.41×10^{13} vg/kg) of SRP-9005 (n = 6/group) confirms γ-sarcoglycan protein expression. Data represent the mean ± SEM. DIA, diaphragm; GAS, gastrocnemius; GLUT, gluteus; HRT, heart; PSO, psoas major; QD, quadriceps; *SGCG*$^{-/-}$, γ-sarcoglycan gene deficient; TA, tibialis anterior; TRI, triceps; WT, wild type.

reaching WT levels in all three dose groups (mean percentage of WT: low dose, 103%; mid dose, 122%; high dose, 120%; Figure 2B).

Loss of SGCG has been shown previously to lead to a concomitant loss of membrane localization by other DAPC proteins, including α-, β-, and δ-sarcoglycan.[3,11] Therefore, we used immunofluorescence staining to determine whether expression of the hSGCG transgene could rescue these other sarcoglycan complex proteins at the sarcolemma. Sarcolemmal localization of α-sarcoglycan (SGCA), β-sarcoglycan (SGCB), and δ-sarcoglycan (SGCD) is absent in *SGCG*$^{-/-}$ mice (0% positive fibers, Figure 3A). Following SRP-9005 treatment, quantitative analysis demonstrated a dose-dependent increase in α-, β-, and δ-sarcoglycan protein production and sarcolemmal localization (mean PPFs at the low, mid, and high dose, respectively, for SGCA: 39%, 61%, 98%; SGCB: 16%, 55%, 92%; SGCD: 13%, 53%, 97%; Figures 3A and 3B). We also observed the same response in heart tissue (Figure S1) with an improvement in the membrane distribution compared with untreated *SGCG*$^{-/-}$ mice. Overall, these data demonstrate dose-dependent recovery of the full sarcoglycan complex, suggesting that SRP-9005 may in turn lead to DAPC restoration at the sarcolemma.

Histology

Consistent with human LGMD 2C/R5, *SGCG*-deficient mice exhibit significant histopathology across all muscles (tibialis anterior and diaphragm muscles as well as heart);[10,11] for example, high levels of central nucleation are evident in *SGCG*$^{-/-}$ mice compared with WT (59%–86% versus 0.5%–3.7%, respectively; Figures 4A and 4B). After SRP-9005 treatment, overall muscle pathology improved, and central nucleation decreased significantly compared with untreated *SGCG*$^{-/-}$ mice for all muscles at the high dose (tibialis anterior, gastrocnemius, quadriceps, triceps, diaphragm, $p < 0.0001$; gluteus, $p = 0.0002$; psoas, $p = 0.011$), and for most at the mid and low doses (tibialis anterior: mid dose, $p = 0.001$; low dose, $p = 0.002$; gastrocnemius, quadriceps, gluteus, diaphragm, mid and low dose, $p < 0.0001$; Figure 4B). Quantitative muscle morphometrics showed an increase in fiber diameter at all three dosages, indicating normalized fiber size similar to WT fibers in tibialis anterior, gastrocnemius, and triceps muscles (Figure 4C and Table S1).

Another common dystrophic feature in patients with LGMD is an increase in fibrosis and adipose tissue due to the degeneration and regeneration of muscle fibers.[32,33] Trichrome staining was used for fibrosis quantification in *SGCG*$^{-/-}$ mice treated with SRP-9005. Disease progression moves from proximal to distal muscles and when analyzing muscle histopathology, it is evident that fibrosis tissue deposition occurs earlier in girdle and proximal muscles than in diaphragm and gastrocnemius muscles, with the diaphragm being more affected in *SGCG*$^{-/-}$ mice, and almost no difference in heart (Figure 5A). After treatment, overall fibrotic tissue deposition improved in both diaphragm and gastrocnemius muscles, with a reduction in fibrosis as dosage escalated compared with levels in untreated *SGCG*$^{-/-}$ mice (Figure 5B). Fibrosis decreased from 13.5% to 5.8% in the gastrocnemius and from 29.3% to 15.7% in the diaphragm of the SRP-9005 mid-dose cohort, compared with the untreated SGCG$^{-/-}$ cohort.

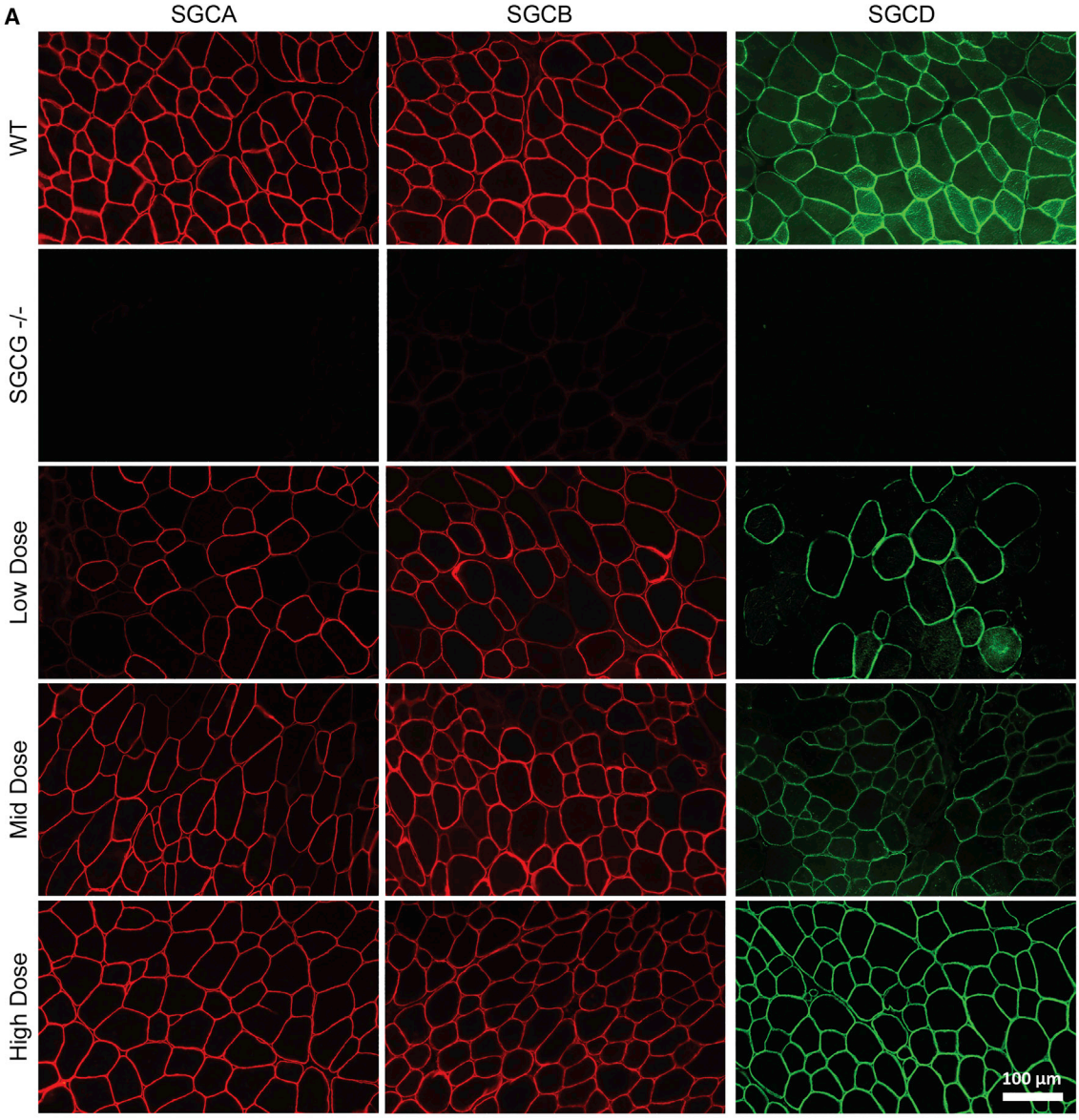

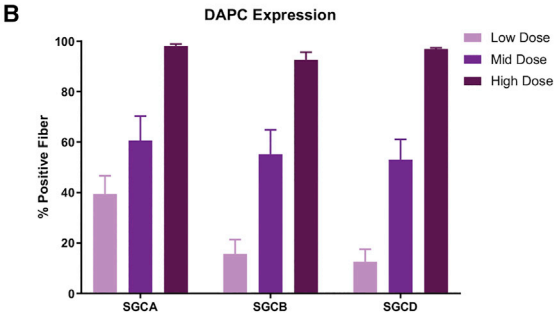

(legend on next page)

Together, these data demonstrate successful systemic delivery of the hSGCG transgene as indicated by robust expression in muscle tissues and improvement in histopathological hallmarks associated with the lack of γ-sarcoglycan protein in *SGCG*$^{-/-}$ mice.

Functional assessments

To determine whether SRP-9005 could provide functional benefit in SGCG-deficient mice, we assessed muscle strength and level of physical activity at 12 weeks post treatment. Deficits in specific force were identified in the tibialis anterior and diaphragm muscles of *SGCG*$^{-/-}$ mice compared with WT (tibialis anterior, p = 0.0001, Figure 6A; diaphragm, p = 0.038, Figure 6B). Mid- and high-dose SRP-9005 treatment significantly improved specific force in both muscles compared with untreated *SGCG*$^{-/-}$ mice (tibialis anterior: low dose p = 0.571, mid dose p = 0.008, high dose p = 0.0001; diaphragm: low dose p = 0.388, mid dose p = 0.088, high dose p = 0.001; Figures 6A and 6B).

A reduction in ambulation and vertical rearing in *SGCG*$^{-/-}$ mice compared with WT controls was observed (ambulation, p = 0.005; vertical activity, p = 0.001; Figure 6C). Laser monitoring of open-field cage activity showed increased ambulation and vertical movement in *SGCG*$^{-/-}$ mice treated with the mid dose of SRP-9005 (ambulation: mid dose versus *SGCG*$^{-/-}$, p = 0.010; vertical activity: mid dose versus *SGCG*$^{-/-}$, p = 0.018). These data show that the delivery of hSGCG restores force production in muscle and physical activity and protects against the breakdown of muscle in *SGCG*$^{-/-}$ mice.

Safety: Creatine kinase and clinical chemistry analysis

Analysis of blood serum chemistries was performed on WT, untreated *SGCG*$^{-/-}$, and treated *SGCG*$^{-/-}$ mice as a measure of safety. Liver enzyme levels (alanine aminotransferase [ALT] and aspartate aminotransferase [AST]) were not increased by SRP-9005 treatment but decreased to WT levels, consistent with a favorable safety profile (Figure 7A). Assessment of serum CK was performed as an analysis of both safety and efficacy. CK is an indicator of destabilized muscle membrane integrity and consequent membrane permeability. Importantly, serum CK levels were significantly reduced in treated groups compared with untreated mice (mean serum CK: untreated *SGCG*$^{-/-}$ 10,185 U/L; mid dose: 3,572 U/L, p = 0.0005; high dose: 253 U/L, p < 0.0001; Figure 7B). Additionally, formalin-fixed tissue sections of all muscles stained with hematoxylin and eosin (H&E) from all cohorts were sent to a veterinary pathologist for formal review of potential toxicity. SRP-9005 administration resulted in no early deaths or macroscopic findings, and there was no evidence of toxicity in any organ noted.

DISCUSSION

This study provides preclinical proof of principle that AAV gene transfer therapy restores γ-sarcoglycan protein expression and leads to histopathological and functional improvements in *SGCG*$^{-/-}$ mice. The highest dose tested, 7.41×10^{13} vg/kg (based on linear plasmid standard titer method), enabled the most robust γ-sarcoglycan expression and effective functional protein restoration.

The development of gene transfer therapies demands a stepwise evaluation of safety, transduction, expression, localization, cellular impact, and functional outcomes. Importantly, we did not observe any adverse effects on non-target tissues. The rAAVrh74 vector provided dose-dependent increases in transduction across skeletal muscles, diaphragm, and heart, demonstrating successful delivery of the transgene into muscle cells with widespread biodistribution. Our results are consistent with previous studies utilizing the rAAVrh74 serotype for successful muscle cell transduction.[12,26,27]

After targeted biodistribution of the transgene was confirmed, we next analyzed γ-sarcoglycan protein production and localization. To drive expression in muscle cells, SRP-9005 contains an MHCK7 promoter, an optimized version of the muscle-specific MCK promoter with enhanced cardiac expression.[28] The MHCK7 promoter has been shown previously to drive robust expression in both skeletal muscle and heart.[12,25,34] Here, immunofluorescence staining demonstrated both robust γ-sarcoglycan protein production across myofibers (nearly 100% positive at the highest dose) and correct localization at the sarcolemma. These results were confirmed by western blot in skeletal, diaphragm, and cardiac muscle in all dose groups where γ-sarcoglycan protein was restored to WT levels at the highest dose in skeletal muscles and heart. Of note, immunofluorescence did show cytoplasmic staining in cardiac tissue from mice in the highest dose cohort. While muscle damage has been observed in a previous report of γ-sarcoglycan overexpression,[35] transgenic animals in this study were genetically induced to overexpress γ-sarcoglycan at 150- to 200-fold WT levels. However, western blot analysis showed that SRP-9005-induced γ-sarcoglycan expression in *SGCG*$^{-/-}$ mice is at or near WT levels at the three doses tested. The observed intracellular staining may instead suggest that SRP-9005 induced high-level γ-sarcoglycan protein expression, resulting in improper trafficking to the sarcolemma following assembly with other sarcoglycans in the Golgi apparatus to form the sarcoglycan complex. However, there is no indication of intracellular γ-sarcoglycan protein aggregates in any of the skeletal muscles, potentially as a result of the differences in stoichiometry and assembly of the sarcoglycan subunits in cardiac versus skeletal muscle.[35] Furthermore, when

Figure 3. Dose-dependent restoration of dystrophin-associated protein complex proteins at the sarcolemma

(A) Sarcolemma expression of α-sarcoglycan, β-sarcoglycan, and δ-sarcoglycan for mice systemically treated with low dose (8.94×10^{10} vg total dose; 4.63×10^{12} vg/kg), mid dose (3.63×10^{11} vg total dose; 1.85×10^{13} vg/kg), or high dose (1.26×10^{12} vg total dose; 7.41×10^{13} vg/kg) of SRP-9005 (n = 6/group) shown in the tibialis anterior muscle. Scale bar, 100 μm. (B) Quantitative analysis of positive fiber DAPC expression. Data represent the mean ± SEM. DAPC, dystrophin-associated protein complex; *SGCG*$^{-/-}$, γ-sarcoglycan gene deficient; WT, wild type.

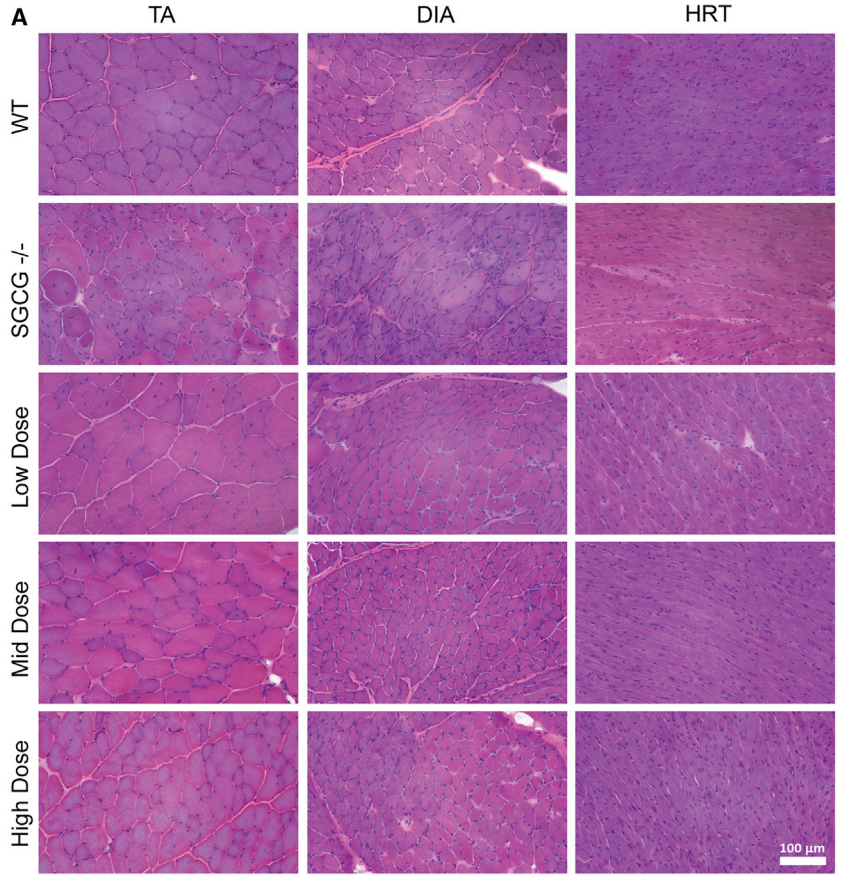

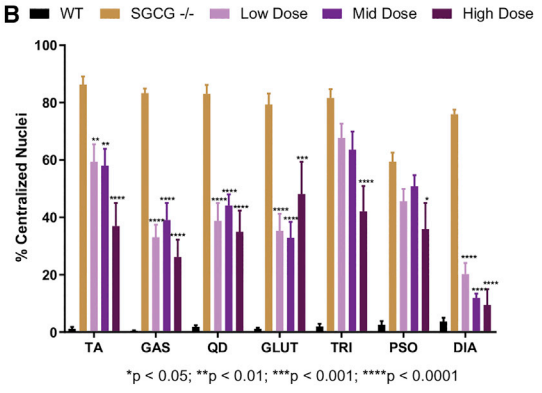

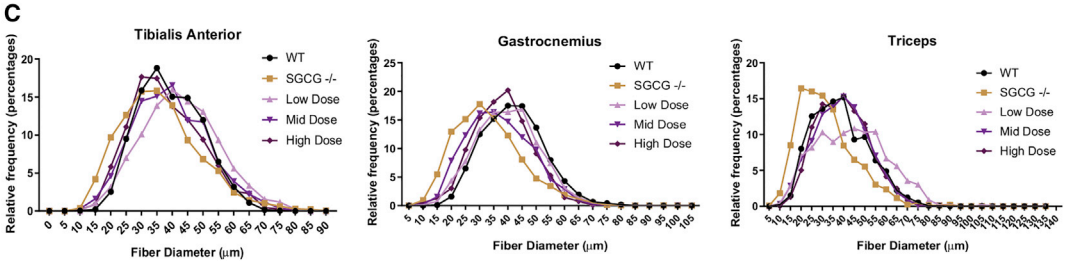

(legend on next page)

staining for the other sarcoglycans, no intracellular aggregation of α-, β-, or δ-sarcoglycan was detected in cardiac tissues with intracellular γ-sarcoglycan staining.

As a component of the sarcoglycan complex, γ-sarcoglycan stabilizes the larger DAPC and contributes to mechanical stabilization of the sarcolemma. Without an intact DAPC, the sarcolemma is vulnerable to damage from the stress of muscle contraction.[36,37] Mutation in any component of the sarcoglycan complex prevents the recruitment and assembly of the other subunits into the complex, as seen by lack of α-, β-, and δ-sarcoglycan expression in *SGCG*$^{-/-}$ mice. Restoration of the sarcoglycan complex within the DAPC is therefore essential for resolving LGMD 2C/R5 phenotypes.[5,7] We demonstrated that rescuing γ-sarcoglycan protein through gene transfer therapy also rescued protein localization at the membrane of the other sarcoglycans in a dose-dependent manner, allowing restoration of the full sarcoglycan complex. Thus, the DAPC can subsequently reassemble and support myofiber integrity during contraction.

Susceptibility to muscle damage due to *SGCG* deficiency often results in skeletal muscle fibrosis. After continuous rounds of degeneration, the muscle tissue is replaced by collagen and other extracellular matrix components, leading to the formation of scar tissue and exacerbation of disease progression.[38] *SGCG*$^{-/-}$ mice have histological features similar to those of patients with LGMD 2C/R5, presenting with high levels of central nucleation, decreased fiber diameter, and fibrosis.[10,11] After treatment with SRP-9005, histopathologic improvements were shown by the return of central nucleation and fiber diameters to WT levels. Fibrosis was also significantly decreased as dosage increased for the gastrocnemius and diaphragm muscles, while in the heart no differences were observed between WT and *SGCG*$^{-/-}$ mice. The histopathological improvements in these muscles corresponded to functional benefits, evidenced by restoration of muscle strength in the tibialis anterior and diaphragm, and increased overall movement shown by improvements in ambulation and vertical rearing activity. Although the number of animals in each group (n = 6) was sufficient to detect dose-dependent improvements in histopathology and function, it should be noted that type I or II statistical errors may still occur.

Functional improvements from baseline were detectable at all doses. We believe that the differences between mid and high dose are related to intrinsic variability in baseline function (i.e., ambulation and vertical activity) observed in the animals. The improvement seen at the higher dose of 7.41 × 10^{13} vg/kg (based on linear plasmid standard for qPCR) is consistent with therapeutic dose levels in other AAV-mediated gene transfer therapy preclinical studies. For example, SGCA has been delivered to *SGCA*$^{-/-}$ mice under control of the tMCK promoter using the rAAVrh74 vector; SGCA expression, DAPC restoration, and corresponding improvements to histopathology and muscle function were shown after a single 1.0–6.0 × 10^{12} vg total dose (based on supercoiled plasmid standard titer method).[27] Similar success using the rAAVrh74 vector[12,26] and MHCK7 promoter[12] was achieved in a model of LGMD 2E/R4 delivering functional β-sarcoglycan to *SGCB*$^{-/-}$ mice. Dose-dependent SGCB expression, DAPC restoration, reduction in central nucleation and fiber degeneration, and functional improvements were achieved using a vector dose of 5 × 10^{13} vg/kg (based on supercoiled plasmid standard titer method).[12,26] This work has since moved to a phase 1/2 clinical trial (n = 6) of systemic gene transfer targeting LGMD 2E/R4. Interim results have shown transgene expression, DAPC restoration, and functional improvements in patients up to 2 years after a single dose of either 1.85 × 10^{13} vg/kg or 7.41 × 10^{13} vg/kg, based on linear plasmid standard for qPCR.[39] Importantly, the clinical trial dosage was consistent with doses that were shown to be effective in preclinical models.

Importantly, there were no adverse clinical abnormalities, and an independent veterinary pathology review found no adverse histopathology in any tissue, including cardiac tissue discussed above. While we did not observe any toxicity or adverse effects related to intracellular γ-sarcoglycan expression in cardiac tissues, we underscore the importance of careful dose titration and further investigation into potential consequences of γ-sarcoglycan overexpression. Additional studies should investigate potential long-term effects of sustained high levels of γ-sarcoglycan expression on cardiac function. Further insight into the molecular mechanisms of sarcoglycan protein transport and assembly may be helpful in understanding the factors that regulate the stoichiometry of the DAPC components. These questions will be addressed in a follow-up study including an in-depth analysis of cardiac function using echocardiogram measurements, and assessment of cardiomyocyte contractility and calcium handling following a high dose of SRP-9005. Additional functional tests, such as treadmill and grip strength analyses, will be performed to assess motor function, muscle strength, and fatigue. A careful examination of cardiac pathology as well as functional improvement will be important for demonstrating safety and efficacy for clinical translation.

In conclusion, our studies of SRP-9005 gene transfer therapy in a mouse model of LGMD 2C/R5 contribute to the growing

Figure 4. Improvement in muscle morphology by SRP-9005 is independent of dose in *SGCG*$^{-/-}$ mice

(A) H&E images of tibialis anterior and diaphragm muscles as well as heart from *SGCG*$^{-/-}$ mice systemically treated with low dose (8.94 × 10^{10} vg total dose; 4.63 × 10^{12} vg/kg), mid dose (3.63 × 10^{11} vg total dose; 1.85 × 10^{13} vg/kg), or high dose (1.26 × 10^{12} vg total dose; 7.41 × 10^{13} vg/kg) of SRP-9005 (n = 6/group). Representative 20× images show a dramatic reduction in centralized nuclei and an overall normalization of fiber size independent of treatment dose. Scale bar, 100 μm. (B) Quantification of centrally located nuclei in left and right muscles (TA, GAS, QD, GLUT, TRI, PSO, DIA) from treated mice compared with *SGCG*$^{-/-}$ and WT controls (n = 6/group; four images per section). Data were analyzed by two-way ANOVA followed by Tukey's multiple comparisons test and represent the mean ± SEM. *p < 0.05, **p < 0.01, ***p < 0.001, ****p < 0.0001 versus *SGCG*$^{-/-}$. (C) Quantification confirming myofiber diameter normalization of tibialis anterior, gastrocnemius, and triceps muscles in vector-treated groups compared with vehicle-treated mice (*SGCG*$^{-/-}$) and WT controls (n = 6/group). DIA, diaphragm; GAS, gastrocnemius; GLUT, gluteus; HRT, heart; PSO, psoas major; QD, quadriceps; *SGCG*$^{-/-}$, γ-sarcoglycan gene deficient; TA, tibialis anterior; TRI, triceps; WT, wild type.

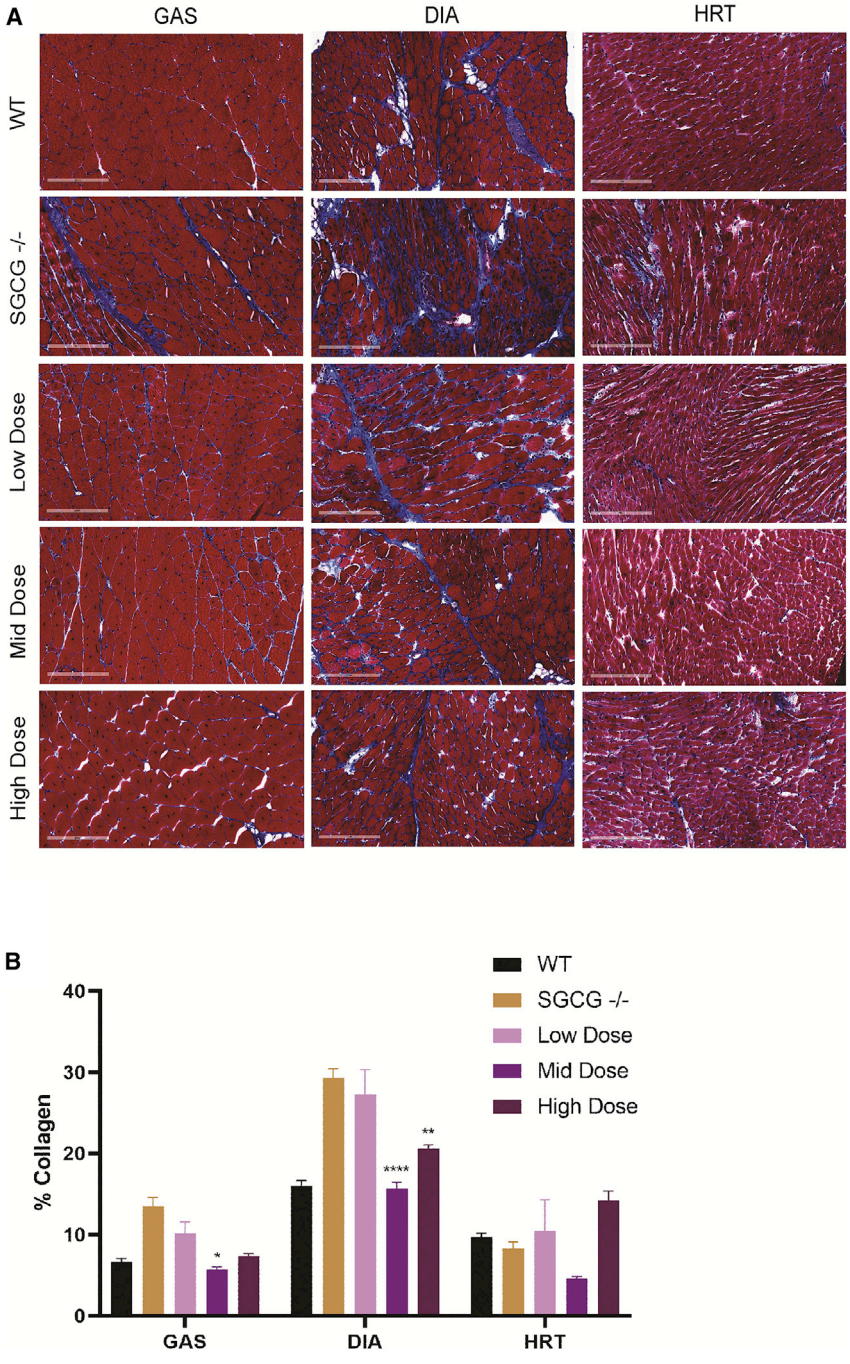

Figure 5. Reduction in fibrosis in *SGCG*$^{-/-}$ mice treated with SRP-9005

(A) Representative images of trichrome staining and (B) quantification of fibrosis in gastrocnemius, diaphragm, and heart muscles from WT mice or *SGCG*$^{-/-}$ mice treated systemically with low dose (8.94×10^{10} vg total dose; 4.63×10^{12} vg/kg), mid dose (3.63×10^{11} vg total dose; 1.85×10^{13} vg/kg), or high dose (1.26×10^{12} vg total dose; 7.41×10^{13} vg/kg) of SRP-9005 (n = 6/group). Data were analyzed by two-way ANOVA followed by Tukey's multiple comparisons test and represent the mean ± SEM. *p < 0.05, **p < 0.01, ***p < 0.001, ***p < 0.0001 versus *SGCG*$^{-/-}$. DIA, diaphragm; GAS, gastrocnemius; HRT, heart; *SGCG*$^{-/-}$, γ-sarcoglycan gene deficient; WT, wild type. Scale bar, 100 μm.

body of evidence for gene replacement therapy in the treatment of sarcoglycanopathies. No clinical studies have been reported to date for systemic gene transfer addressing LGMD 2C/R5. These preclinical results inform the establishment of a minimal effective dose for future clinical studies of SRP-9005 gene transfer in patients and provide support for advancing SRP-9005 to clinical development for the treatment of LGMD 2C/R5.

MATERIALS AND METHODS

Animal models

All procedures were conducted in accordance with approval by The Sarepta Genetic Therapies Center of Excellence Institutional Animal Care and Use Committee. WT (C57BL/6J) mice and *SGCG*$^{-/-}$ mice, with BL6 genetic background, were bred and maintained as homozygous animals under standardized conditions in the Animal Resources Core at the Sarepta Genetic Therapies Center of Excellence.

Mice were maintained on Teklad Global Rodent Diet (3.8% fiber, 18.8% protein, 5% fat chow) with a 12:12-h dark/light cycle. All animals were housed in standard mouse cages with food and water *ad libitum*. For all experiments, mice from both sexes were used: WT (n = 6, 5 male [M]/1 female [F]); untreated *SGCG*$^{-/-}$ (n = 6, 4 M/2 F); low dose (n = 6, 6 M/0 F); mid dose (n = 6, 4 M/2 F); high dose (n = 6, 0 M/6 F).

Genotyping

Standard PCR of isolated DNA was used to identify *SGCG*$^{-/-}$ mice. DNA from tail clippings was isolated and analyzed by PCR using OneTaq DNA Polymerase (New England Biolabs, Ipswich, MA). A series of primers was used in the PCR analysis to determine the *SGCG*$^{-/-}$ status. The following primers and conditions were used: GGA GGA AGC GCT GCC TAT ACC TAT T; CAA ATG CTT GCC TCA GGT ATT TC; GCC TGC TCT TTA CTG AAG GCT CTT T.[11] Reactions were carried out on genomic DNA for 30 cycles under the following conditions: 94°C, 30 s; 58°C, 30 s; 68°C, 25 s; followed by 5 min at 68°C.

hSGCG gene construction and vector production

The full-length human SGCG cDNA (NC_000013.11) was codon-optimized and used in the design of the gene therapy construct.

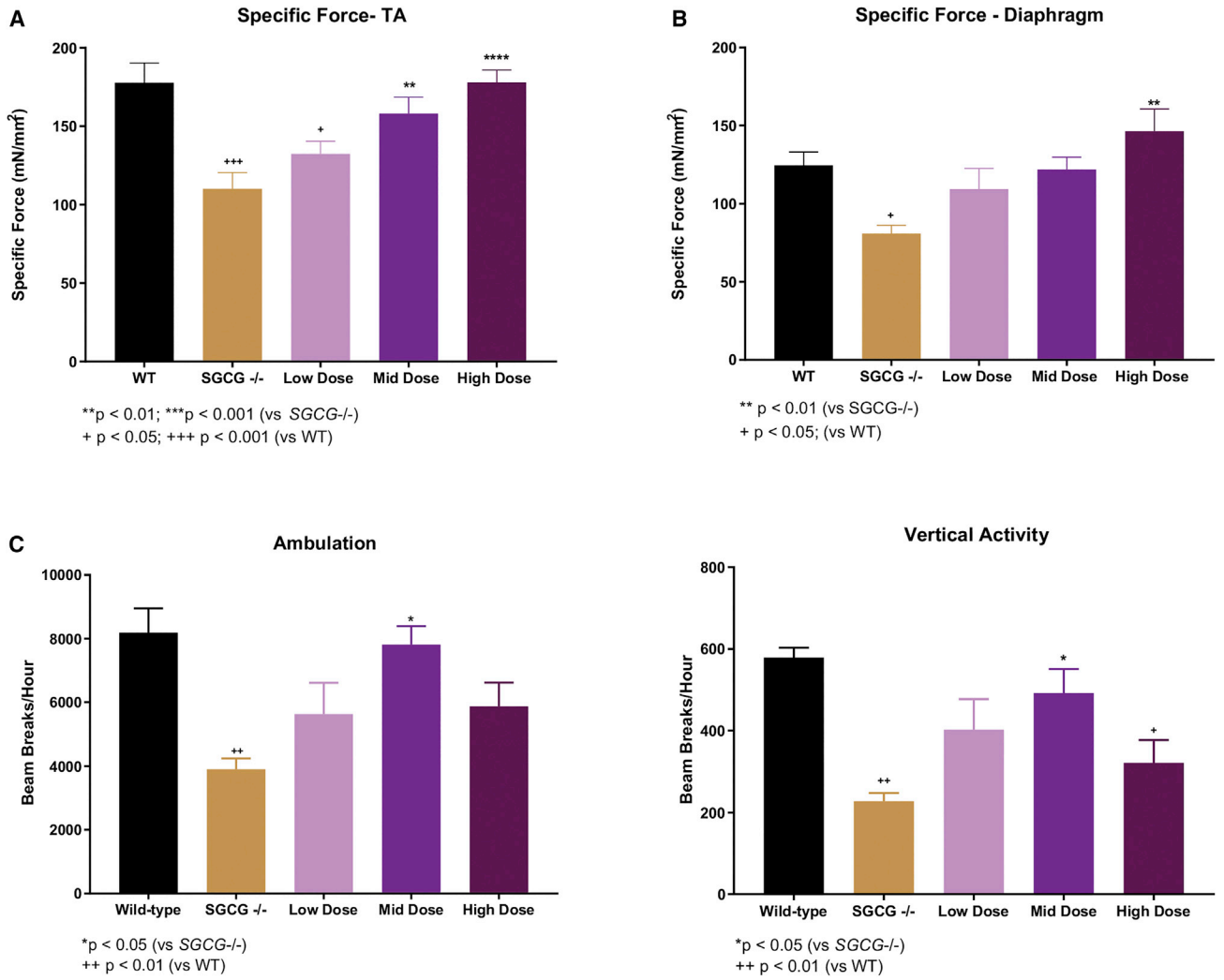

Figure 6. Functional benefits in *SGCG*$^{-/-}$ mice treated with SRP-9005

(A) Following 12 weeks of SRP-9005 treatment, specific force of tibialis anterior muscles (both left and right) was measured (data were normalized to tibialis anterior weight). Specific force increased in all SRP-9005-treated *SGCG*$^{-/-}$ mice (with minimal difference between doses) compared with vehicle-treated (*SGCG*$^{-/-}$) and WT mice (n = 6/group, average of both legs used for analysis [total n = 12]). (B) Diaphragm muscle strips were harvested to measure specific force. Following 12 weeks of SRP-9005 treatment, the force was significantly increased in treated mice compared with *SGCG*$^{-/-}$ and WT mice. (C) Following 12 weeks of treatment, improvement was seen in analysis of activity cage ambulation and vertical activity through open-field analysis in vector-treated mice compared with *SGCG*$^{-/-}$ and WT mice (n = 6/group). One-way ANOVA with Tukey's multiple comparisons test was performed for analysis of tibialis anterior and diaphragm physiology and for analysis of cage activity. Data represent the mean ± SEM. *p < 0.05, **p < 0.01, ***p < 0.001 versus *SGCG*$^{-/-}$; $^{+}$p < 0.05, $^{++}$p < 0.01, $^{+++}$p < 0.001 versus WT. *SGCG*$^{-/-}$, γ-sarcoglycan gene deficient; WT, wild type.

The cassette includes a consensus Kozak sequence (CCACC), an SV40 chimeric intron, and synthetic polyadenylation site (53 bp). The muscle-specific MHCK7 promoter is used to drive expression. This promoter is well established for enhancing cardiac and diaphragm transgene expression.[12,13] The hSGCG expression cassette was cloned between AAV2 ITRs, and the cassette was packaged into an rAAVrh74 vector using a triple transfection method in the Vector Manufacturing Facility in the Center for Gene Therapy at Nationwide Children's Hospital, as previously described.[13,40,41]

TaqMan qPCR was used to titer the vector using a primer probe set located in the MHCK7 promoter region. A linearized plasmid standard containing the same MHCK7 target sequence was used to generate the standard curve for the assay. There were no alterations from standard AAV production and purification using this approach.

Treatment cohorts

SRP-9005 was administered systemically via injection of vector into the tail vein of three separate doses of vector or saline in a

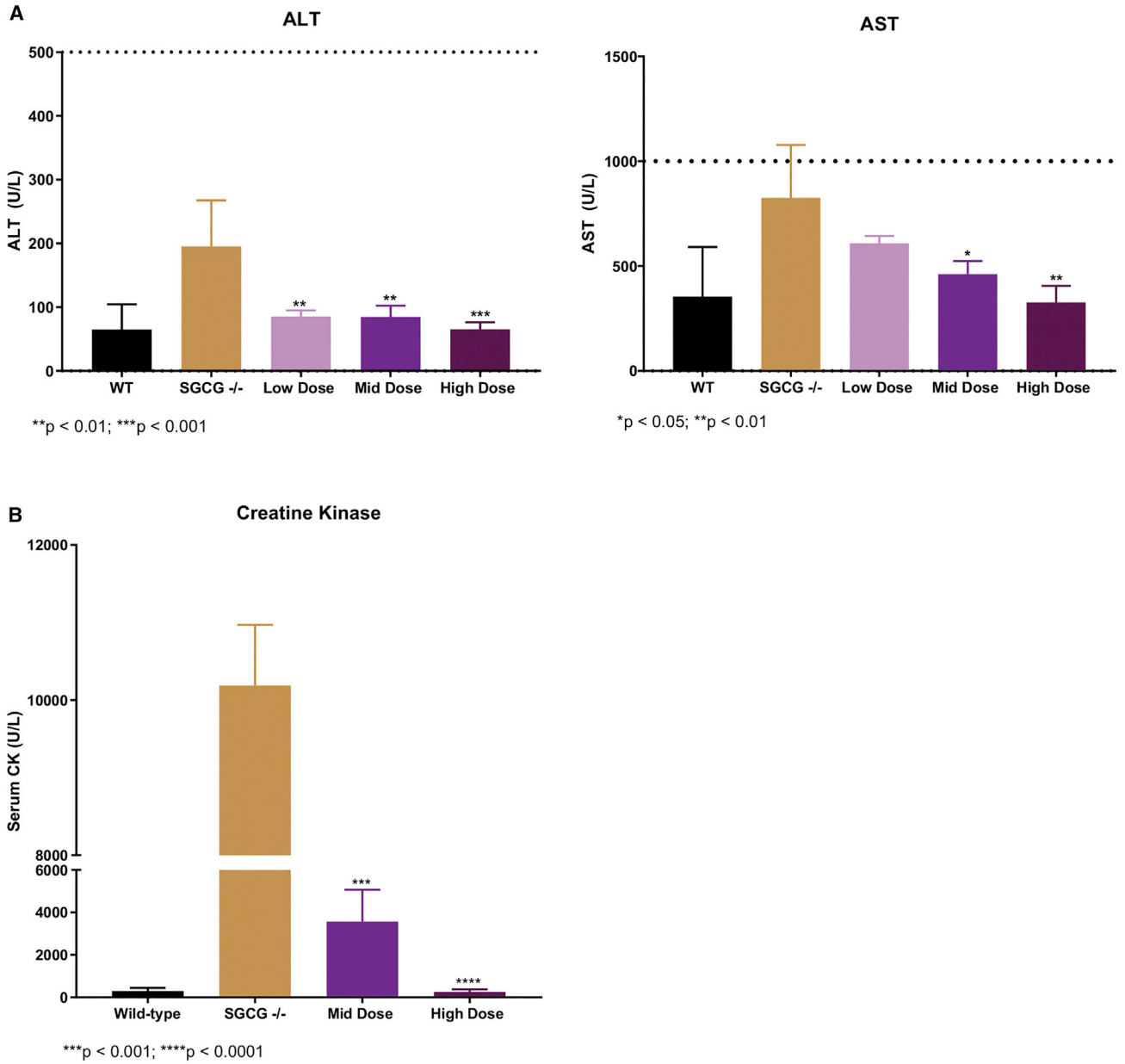

Figure 7. Serum chemistries

(A) Liver enzyme (ALT and AST) levels were analyzed for toxicity (n = 6/group). Dotted lines indicate normal limits in WT mice. (B) CK levels in serum decreased in all treated groups compared with untreated *SGCG*$^{-/-}$ and WT controls; mid and high doses only (low-dose data were not collected due to insufficient sample volume). Data were analyzed by one-way ANOVA for all blood chemistries and represent the mean ± SEM. ALT, alanine aminotransferase; AST, aspartate aminotransferase; CK, creatine kinase; *SGCG*$^{-/-}$, γ-sarcoglycan gene deficient; WT, wild type.

dose-escalation study. Vector dose calculated based on linear qPCR. Four-week-old *SGCG*$^{-/-}$ mice were injected with the low (8.94×10^{10} vg total dose; 4.63×10^{12} vg/kg; n = 6, 6 M/0 F), mid (3.63×10^{11} vg total dose; 1.85×10^{13} vg/kg; n = 6, 4 M/2 F), or high (1.26×10^{12} vg total dose; 7.41×10^{13} vg/kg; n = 6, 0 M/6 F) dose of SRP-9005. Additionally, WT mice (n = 6, 5 M/1 F) and *SGCG*$^{-/-}$ control mice (n = 6, 4 M/2 F) were injected with saline. Mice were injected at 4–5 weeks of age and euthanized approximately 12 weeks after gene delivery.

Tissue processing

Skeletal muscles were extracted from each mouse, placed on saline-dampened gauze, then placed on cryogel mounted wooden chucks and fresh frozen in cooled 2-methylbutane. Organs were

bisected and one half placed in 10% neutral buffered formalin followed by paraffin embedding for sectioning and H&E staining. The other half of the organ was fresh frozen for subsequent molecular studies.

Biodistribution qPCR analysis

The presence of test article-specific DNA sequences in muscles and organs were evaluated using a real-time qPCR assay with a vector-specific primer probe set designed to amplify a sequence in the MHCK7 promoter (n = 3 per low-, mid-, and high-dose group). Frozen tissues were sectioned using a cryostat (15 sections at 20 μm thickness) into a prechilled microcentrifuge tube. Genomic DNA was isolated using a DNeasy Blood & Tissue Kit (QIAGEN, Hilden, Germany) according to the manufacturer's protocol. The resulting DNA samples were stored at −80°C until analysis. Test DNA was prepared by diluting each sample to 10 ng/μL in nuclease-free water (Thermo Fisher, catalog no. [#]AM9906). Standards were prepared using linearized plasmid, starting at a concentration of 1×10^6 copies/μL and serially diluted to 10 copies/μL. All samples and standards were analyzed in triplicate. Cycling was performed by an initial denaturing step at 95°C for 20 s followed by 40 cycles of 95°C for 1 s and 60°C for 30 s. QuantStudio system and software were used to run qPCR. The following primers and probe were used in the study: MHCK7 forward primer 5′-CCA ACA CCT GCT GCC TCT AAA-3′, MHCK7 reverse primer 5′-GTC CCC CAC AGC CTT GTT C-3′, and MHCK7 probe 5′-TGG ATC CCC TGC ATG CGA AGA TC-3′ (5′ 6-FAM, 3′ Iowa Black FQ, Internal ZEN Quencher [Integrated DNA Technologies]). The primers and probe were diluted to final concentrations of 100 nM, 100 nM, and 200 nM per reaction, respectively. The standard curve was used to calculate the number of copies in each reaction. To determine the number of vector genome copies per nucleus, the following equation was used:

$$\text{Copies per nucleus} = 10\text{^}((\text{CT} - \text{Std Curve y Intercept}) / \text{Std Curve Slope}) \times (1{,}000 / \text{Amount loaded per well (ng)}) \times (5.98 \times 10^{-6}).$$

Immunofluorescence

Protein production across muscle tissues and DAPC restoration was assessed using immunofluorescence. Cryosections (12 μm thickness) from the tibialis anterior, gastrocnemius, quadriceps, psoas major, gluteus, triceps, diaphragm, and heart muscles were subjected to immunofluorescence protein staining via our previously used protocol.[26] For γ-sarcoglycan protein detection, sections were incubated with a γ-sarcoglycan rabbit polyclonal primary antibody (Novus, #NBP1-59744) at a dilution of 1:100. For α-, β-, and δ-sarcoglycan protein detection, sections were incubated with an α-sarcoglycan rabbit polyclonal antibody (Abcam, #ab189254, diluted 1:100), β-sarcoglycan mouse monoclonal antibody (Leica, #B-SARC-L-CE, diluted 1:100), and δ-sarcoglycan rabbit monoclonal antibody (Abcam, #ab137101, diluted 1:50), respectively. Four random 20× images covering the four different quadrants of the muscle section were taken using Gryphax software (2.0.0.68) with a Jenoptik Prokyon camera mounted on a Nikon Eclipse Ni-U microscope. The percentage of fibers positive for α-, β-, δ-, and γ-sarcoglycan protein staining compared with controls (WT normalized to 100% and *SGCG*$^{-/-}$ as effectively 0%) was determined for each image and averaged for each muscle. Fibers counted were defined by the structural appearance of the fiber's cross-section. To facilitate scoring, National Institutes of Health (NIH) ImageJ software with the Cell Counter plugin was used to count total fibers. Positive fiber expression was defined as having at least 50% of the fiber staining brighter than the vehicle-treated *SGCG*$^{-/-}$ saline controls, as previously described.[26] Positive fibers were scored based on the original image exposure; there was no adjustment to the brightness or contrast of any image during the positive image scoring process. The remaining fibers were scored as negative. The test article was blinded at the time of injection. The operator who conducted the injections did not perform any analysis outside of the injection. There is no expression or residual protein in the untreated group, so it is clear which animal received treatment and which did not when observing under the microscope, leaving blinding irrelevant for immunofluorescence quantification. To mitigate variability in intensity, images were taken at the same exposure. Quantification data of immunofluorescent-positive fibers expressing α-, δ-, and γ-sarcoglycan proteins are reported as mean ± SEM, with six mice per treatment group.

Western blot analysis

Tissue sections (20 μm thickness, 15 sections) were collected into a microcentrifuge tube and homogenized with 150 μL of homogenization buffer (125 mM Tris-HCl, 4% SDS, 4 M urea) in the presence of one protease inhibitor cocktail tablet. After homogenization, the samples were centrifuged at 10,000 rpm for 10 min at 4°C, and the resulting supernatant was collected. Protein concentration was determined using the NanoDrop. Protein samples (20 μg) were electrophoresed on a 3%–8% polyacrylamide Tris-acetate gel for 70 min at 150 V, then transferred onto a polyvinylidene fluoride membrane for 90 min at 35 V. The membrane was blocked in 5% non-fat dry milk in TBST (Tris-buffered saline with Tween 20) for 1 h, and then incubated in a 1:2,000 dilution of a monoclonal rabbit γ-sarcoglycan antibody (Abcam, #ab203113) and a 1:50,000 dilution of a mouse α-actinin antibody (Sigma, #A7811). Anti-mouse (Sigma, #AP308P) and anti-rabbit secondary horseradish peroxidase antibodies (Invitrogen, #65-6120) were used for ECL immunodetection. Western blot detection and quantification were performed using the Alliance Q9 Advanced chemiluminescence imaging system and software. Auto-capture mode was used to set the exposure time, which varied depending on the intensity of the sample. The volumes of the protein bands were quantified as the sum of all the pixel intensities included in the defined area using the analysis mode of the software and normalized to the corresponding loading control bands. Relative protein expression was determined by dividing by the WT volume ratios.

Morphometric analysis

H&E staining was performed to visualize muscle morphology, including fiber size and central nucleation, on cryosections of muscle (12 μm thickness) from 16-week-old WT mice (n = 6), *SGCG*$^{-/-}$ mice (n = 6), and SRP-9005-treated *SGCG*$^{-/-}$ mice (n = 6 per dose, 12 weeks post treatment). The percentage of myofibers with central nucleation was determined in the tibialis anterior, gastrocnemius, quadriceps, gluteus, triceps, psoas major, and diaphragm muscles. Additionally, muscle fiber diameters were measured using Feret's diameter in the tibialis anterior, triceps, and gastrocnemius muscles. There was a range of 1,600–2,000 fibers quantified per muscle from each treatment group and from the control cohort. Four random 20× images per muscle per animal were taken using Gryphax software (2.0.0.68) with a Jenoptik Prokyon camera mounted on a Nikon Eclipse Ni-U microscope. Centrally nucleated fibers were quantified using NIH ImageJ software, and fiber diameters were measured using Zeiss Axiovision LE4 software.

Histopathology

At necropsy, muscles (tibialis anterior, gastrocnemius, quadriceps femoris, gluteus maximus, psoas major, triceps brachii, diaphragm, and heart) and select organs were formalin-fixed, embedded in paraffin, sectioned, and stained with H&E. The resulting slides from all animals were forwarded to Histo-Scientific Research Laboratories for formal review by a veterinary pathologist.

Masson's trichrome stain for fibrosis quantification

Frozen muscle tissue sections (12 μm) were mounted on Fisherbrand Superfrost charged microscope slides. Slides were fixed in 10% neutral buffered formalin (Fisher, #SF100-4) for 10 min and rinsed in deionized water (Fisher, #W2-4). Slides were placed in 95% reagent alcohol (Fisher, #HC13001GL) and allowed to air dry for 15 min, then fixed in Bouin's fixative for 32 min and washed with tap water followed by distilled water until clear. Slides were then incubated in Weigert's iron hematoxylin solution for 5 min and washed in running water for 5 min, followed by rinsing in distilled water before being placed in Biebrich's scarlet-acid fuchsin for 2 min and washed again in distilled water. Slides were then transferred to phosphotungstic-phosphomolybdic acid for 10 min, placed in aniline blue for 5 min, and washed thoroughly with distilled water. After incubation in 1% aqueous acetic acid for 5 min, the slides were quickly dehydrated in two changes of 95% reagent alcohol followed by two changes of 100% alcohol (Fisher, #HC-800-iGAL). Slides were then transferred to xylene (Fisher, #X3P-1GAL) and cleared in three changes before being mounted with glass coverslips using Cytoseal 60 medium (Thermo Fisher, #8310). Bouin's fixative, Weigert's iron hematoxylin A and B, Biebrich's scarlet-acid fuchsin, phosphotungstic-phosphomolybdic acid, aniline blue, and 1% acetic acid aqueous were all part of Masson's trichrome kit (Poly Scientific, #k037). Full-slide scans of the Masson's trichrome staining were prepared using the Aperio VERSA 200 Imaging System (Leica Biosystems Imaging) and analyzed for percentage of collagen quantification. Analysis was performed using Aperio ImageScope software (v12.4.3.5008). Images were first annotated to select regions of interest and to remove artifacts (i.e., tissue folding, longitudinal fibers, fat) that would yield inaccurate results. The positivity of blue chromogen (ratio of blue stain to red stain) was detected using the Positive Pixel Count v9 algorithm on ImageScope and reported as a percentage to denote the collagen content in the annotated areas. Results from the left and right gastrocnemius images were averaged for each animal.

Formulas:

$$\text{Positivity of blue chromogen} = \frac{\text{Number of blue pixel count}}{\text{Number of blue pixel count} + \text{Number of red pixel count}},$$

where blue pixel count corresponds to collagen area and red pixel count corresponds to non-collagen muscle area.

$$\%\ \text{Collagen} = \text{Positivity of blue chromogen} \times 100.$$

Tibialis anterior tetanic contraction for functional assessment

The tibialis anterior assessment procedure followed the protocol listed in Hakim et al.[42] Mice were anesthetized with ketamine/xylazine mixture (137.5 mg/kg and 10 mg/kg, respectively) administered intraperitoneally. The hindlimb skin was removed to expose the tibialis anterior muscle and patella. The length of muscle is measured after dissection, prior to placement of the mouse, and the length is entered into the software. Care was taken to limit drying of the exposed muscle by constantly hydrating the exposed muscles with a saline-dampened Kimwipe drape. The tibialis anterior distal tendon was then dissected out (left and right side per animal; average of both legs used for analysis [n = 12 per cohort]), and a double square knot was tied around the tendon with 4-0 suture as close to the muscle as possible before cutting the tendon. Mice were then transferred to a thermal controlled platform and maintained at 37°C. To stabilize the leg, a metal pin was placed behind the patellar tendon, and the knee was secured to the platform with the tibialis anterior distal tendon sutured to the level arm of the force transducer (Aurora Scientific, Aurora, Canada). An electrode was placed near the sciatic nerve to stimulate it. A warm-up protocol designed by Aurora Scientific was initiated whereby the resting tension was set at 3–4 *g* force and maintained for 5 min, muscle stimulation at 1 Hz (three times, 30 s apart), and an additional muscle stimulation at 150 Hz (three times, 60 s apart). Once the muscle was stabilized, the resting tension was set to a length (optimal length) where twitch contractions were maximal. After a 3-min rest period, the tibialis anterior muscle was stimulated at 50, 100, 150, and 200 Hz, allowing a 1-min rest between each stimulus. Following a 5-min rest, the muscles were subjected to a series of ten isometric contractions, occurring at 1-min intervals with a 10% stretch-lengthening procedure. The duration of tetanic contraction lasts 200 ms. After the eccentric contractions the mice were euthanized, and both tibialis anterior muscles were dissected and frozen for histology and molecular studies.

Formulas:

$$\text{Tibialis anterior limb} - \text{specific force} = \text{absolute force} / \text{cross sectional area}$$

$$\text{Absolute force} = \text{Force at 150 Hz} \times 9.8\ (9.8\ \text{mN} = 1\ \text{g})$$

$$\text{Cross} - \text{sectional area} = \text{muscle weight (mg)} / [1.06\ (\text{mg} / \text{mm}^3) \times \text{muscle length (mm)} \times 0.6]$$

Diaphragm tetanic contraction for functional assessment

Mice were euthanized, and the diaphragm was dissected with rib attachments and central tendon intact and placed in Krebs-Henseleit (K-H) buffer (118 mM NaCl, 4.7 mM KCl, 1.2 mM $MgSO_4$, 1.25 mM $CaCl_2$, 1.2 mM KH_2PO_4, 25 mM $NaHCO_3$, 11 mM glucose) as previously described.[43–45] A 2- to 4-mm-wide section of diaphragm was isolated per animal per cohort (n = 6). Diaphragm strips were tied firmly with braided surgical silk (6-0; Surgical Specialties, Reading, PA) at the central tendon and sutured through a portion of rib bone affixed to the distal end of the strip. Each muscle was transferred to a water bath filled with oxygenated K-H solution that was maintained at 37°C. The muscles were aligned horizontally and tied directly between a fixed pin and a dual-mode force transducer-servomotor (305C; Aurora Scientific). Two platinum plate electrodes were positioned in the organ bath to flank the length of the muscle. The muscle was stretched to optimal length for measurement of twitch contractions and then allowed to rest for 10 min before initiation of the tetanic protocol. Once the muscle was stabilized, it was set to an optimal length of 1 g and subjected to a warm-up, which consisted of three 1-Hz twitches every 30 s followed by three 150-Hz twitches every minute. After a 3-min rest period, the diaphragm was stimulated at 20, 50, 80, 120, 150, and 180 Hz, allowing a 2-min rest period between each stimulus, each with a duration of 250 ms to determine maximum tetanic force. Muscle length and weight were measured, and the force was normalized for muscle weight and length.

Formulas:

$$\text{Diaphragm} - \text{specific force} = \text{absolute force at 150 Hz} / \text{cross sectional area}$$

$$\text{Absolute force} = \text{force at 150 Hz} \times 9.8\ (9.8\ \text{mN} = 1\ \text{g})$$

$$\text{Cross sectional area} = \text{muscle weight (mg)} / [1.06\ (\text{mg} / \text{mm}^3) \times \text{diaphragm fiber length (mm)} \times 1]$$

Laser monitoring of open-field cage activity

SGCG$^{-/-}$ and WT mice were subjected to an open-field activity protocol similar to that used in previous reports.[43,46] An open-field activity chamber was used to determine the overall activity of the experimental mice. Mice at 4 weeks of age from the WT (n = 6, 5 M/1 F) and untreated *SGCG*$^{-/-}$ (n = 6, 4 M/2 F) control groups, along with SRP-9005-treated *SGCG*$^{-/-}$ mice (low dose [n = 6, 6 M/0 F]; mid dose [n = 6, 4 M/2 F]; high dose [n = 6, 0 M/6 F]) were subjected to analysis following a previously described protocol[43,46] with several modifications. Mice were treated with SRP-9005 at 4 weeks of age, with an endpoint activity assessment of 12 weeks post treatment. Cohorts were injected 1 week apart from each other to eliminate variability in endpoint age. Sessions were broken down by cohort. All mice were tested at the same time of day, between the hours of 06:10 and 08:30, when mice are most active. All mice were tested in an isolated room under dim light and with the same handler each time. To reduce anxiety and minimize behavioral variables that could potentially affect normal activity of the mice and, consequently, the results of the assay, we tested mice that were not individually housed.[47] Mouse activity was monitored using the Photobeam activity system (San Diego Instruments, San Diego, CA). This system uses a grid of invisible infrared light beams that traverse the animal chamber front to back and left to right to monitor the position and movement of the mouse within an x-y-z plane. Activity was recorded for 1-h cycles at 5-min intervals. Mice were acclimatized to the activity test room for an initial 1-h session 3 and 4 days before data acquisition began. Mice were tested in individual chambers. The testing equipment was cleaned between each use to reduce mouse reactionary behavioral variables that could alter results. The data were converted to a Microsoft Excel worksheet, and all calculations were done within the Excel program. Individual beam breaks for movement in the x and y planes were added up for each mouse to represent total ambulation, and beam breaks in the z plane were added up to obtain vertical activity within the 1-h time interval.

Serum chemistry and hematology

As a measure of safety, blood chemistries and hematology studies were performed on vector-dosed *SGCG*$^{-/-}$ and WT mice. Whole blood was retrieved from cardiac puncture from treated WT and *SGCG*$^{-/-}$ mice. Blood was collected in a serum-separating tube and centrifuged for 10 min at 3,500 rpm. Serum was collected, frozen, and sent to Nationwide Children's Hospital for processing and assessment of AST and ALT liver enzyme levels.

Serum creatine kinase measurement

Levels of CK were measured in the sera of WT mice (n = 6), untreated *SGCG*$^{-/-}$ lactated Ringer's solution (LR)-treated mice (n = 6), and SRP-9005-treated *SGCG*$^{-/-}$ mice at mid and high doses (n = 6) (low-dose data were not collected due to insufficient sample volume) using the CK SL Assay according to manufacturer's protocol (Sekisui Diagnostics, Charlottetown, PE, Canada; #326-10). In brief, 25 μL of serum was mixed with 1 mL of the working reagents and added to a cuvette. A kinetic assay was set on the spectrophotometer to measure the absorbance at 340 nm every 30 s for 180 s. CK levels were calculated using the absorbance readings and the equation

$$\mathbf{U}/\mathbf{L} = [(\triangle \text{Abs.}/\text{min}) \times 1.025 \times 1,000]/[1 \times 6.22 \times 0.025] = (\triangle \text{Abs.}/\text{min}) \times 6,592.$$

Statistical analysis

Statistical analysis was performed using GraphPad Prism 7.01 software. Data were expressed as the mean ± SEM (error bars). One-way ANOVA with Tukey's multiple comparisons test was performed for analysis of blood chemistries, serum CK, diaphragm and tibialis anterior physiology, and cage activity. Two-way ANOVA with Tukey's multiple comparisons test was performed for analysis of central nucleation. Kruskal-Wallis test with Dunn's multiple comparisons test was performed for analysis of fiber diameter.

DATA AVAILABILITY

Qualified researchers may request access to the data that support the findings of this study from Sarepta Therapeutics by contacting medinfo@sarepta.com.

SUPPLEMENTAL INFORMATION

Supplemental information can be found online at https://doi.org/10.1016/j.omtm.2023.01.004.

ACKNOWLEDGMENTS

This study was funded by Sarepta Therapeutics. Medical writing support was provided by Lucia Quintana-Gallardo, PhD, of Sarepta Therapeutics, and Kristin M. Allan, PhD, of Eloquent Scientific Solutions, and funded by Sarepta Therapeutics. The work presented was completed at the Genetic Therapies Center of Excellence in Columbus, Ohio, USA.

AUTHOR CONTRIBUTIONS

Y.-E.S. performed data collection, analysis and interpretation of results, and draft manuscript preparation. S.H.B., A.N.K., O.C.R., K.A., A.H., and E.L.P. performed data collection, analysis, and interpretation of results. S.L. and D.A.G. carried out the study design and review, and interpretation of results. R.A.P. was responsible for interpretation of results and manuscript preparation. L.R.R.-K. and E.R.P. were responsible for the study conception and design, and review, interpretation of results, and manuscript preparation.

DECLARATION OF INTERESTS

The authors are employees of the study sponsor, Sarepta Therapeutics, Inc., and may own stock/options in the company.

REFERENCES

1. Liewluck, T., and Milone, M. (2018). Untangling the complexity of limb-girdle muscular dystrophies. Muscle Nerve *58*, 167–177. https://doi.org/10.1002/mus.26077.

2. Murphy, A.P., and Straub, V. (2015). The classification, natural history and treatment of the limb girdle muscular dystrophies. J. Neuromuscul. Dis. *2*, S7–S19. https://doi.org/10.3233/JND-150105.

3. McNally, E.M. (2013). The sarcoglycans. In Madame Curie Bioscience Database, https://www.ncbi.nlm.nih.gov/books/NBK6317/.

4. Taghizadeh, E., Rezaee, M., Barreto, G.E., and Sahebkar, A. (2019). Prevalence, pathological mechanisms, and genetic basis of limb-girdle muscular dystrophies: a review. J. Cell. Physiol. *234*, 7874–7884. https://doi.org/10.1002/jcp.27907.

5. Chu, M.L., and Moran, E. (2018). The limb-girdle muscular dystrophies: is treatment on the horizon? Neurotherapeutics *15*, 849–862. https://doi.org/10.1007/s13311-018-0648-x.

6. Marsolier, J., Laforet, P., Pegoraro, E., Vissing, J., and Richard, I.; Sarcoglycanopathies Working Group (2017). 1st international workshop on clinical trial readiness for sarcoglycanopathies 15-16 november 2016, evry, France. Neuromuscul. Disord. *27*, 683–692. https://doi.org/10.1016/j.nmd.2017.02.011.

7. Wicklund, M.P., and Kissel, J.T. (2014). The limb-girdle muscular dystrophies. Neurol. Clin. *32*, 729–749. https://doi.org/10.1016/j.ncl.2014.04.005.

8. Fayssoil, A., Ogna, A., Chaffaut, C., Chevret, S., Guimarães-Costa, R., Leturcq, F., Wahbi, K., Prigent, H., Lofaso, F., Nardi, O., et al. (2016). Natural history of cardiac and respiratory involvement, prognosis and predictive factors for long-term survival in adult patients with limb girdle muscular dystrophies type 2C and 2D. PLoS One *11*, e0153095. https://doi.org/10.1371/journal.pone.0153095.

9. Barton, E.R., Pacak, C.A., Stoppel, W.L., and Kang, P.B. (2020). The ties that bind: functional clusters in limb-girdle muscular dystrophy. Skelet. Muscle *10*, 22. https://doi.org/10.1186/s13395-020-00240-7.

10. Demonbreun, A.R., Wyatt, E.J., Fallon, K.S., Oosterbaan, C.C., Page, P.G., Hadhazy, M., Quattrocelli, M., Barefield, D.Y., and McNally, E.M. (2019). A gene-edited mouse model of limb-girdle muscular dystrophy 2C for testing exon skipping. Dis. Model. Mech. *13*, dmm040832. https://doi.org/10.1242/dmm.040832.

11. Hack, A.A., Ly, C.T., Jiang, F., Clendenin, C.J., Sigrist, K.S., Wollmann, R.L., and McNally, E.M. (1998). Gamma-sarcoglycan deficiency leads to muscle membrane defects and apoptosis independent of dystrophin. J. Cell Biol. *142*, 1279–1287. https://doi.org/10.1083/jcb.142.5.1279.

12. Pozsgai, E.R., Griffin, D.A., Heller, K.N., Mendell, J.R., and Rodino-Klapac, L.R. (2017). Systemic AAV-mediated beta-sarcoglycan delivery targeting cardiac and skeletal muscle ameliorates histological and functional deficits in LGMD2E mice. Mol. Ther. *25*, 855–869. https://doi.org/10.1016/j.ymthe.2017.02.013.

13. Mendell, J.R., Sahenk, Z., Lehman, K., Nease, C., Lowes, L.P., Miller, N.F., Iammarino, M.A., Alfano, L.N., Nicholl, A., Al-Zaidy, S., et al. (2020). Assessment of systemic delivery of rAAVrh74.MHCK7.micro-dystrophin in children with duchenne muscular dystrophy: a nonrandomized controlled trial. JAMA Neurol. *77*, 1122–1131. https://doi.org/10.1001/jamaneurol.2020.1484.

14. Nelson, C.E., Wu, Y., Gemberling, M.P., Oliver, M.L., Waller, M.A., Bohning, J.D., Robinson-Hamm, J.N., Bulaklak, K., Castellanos Rivera, R.M., Collier, J.H., et al. (2019). Long-term evaluation of AAV-CRISPR genome editing for Duchenne muscular dystrophy. Nat. Med. *25*, 427–432. https://doi.org/10.1038/s41591-019-0344-3.

15. Mosqueira, M., Zeiger, U., Förderer, M., Brinkmeier, H., and Fink, R.H.A. (2013). Cardiac and respiratory dysfunction in Duchenne muscular dystrophy and the role of second messengers. Med. Res. Rev. *33*, 1174–1213. https://doi.org/10.1002/med.21279.

16. DiMattia, M.A., Nam, H.J., Van Vliet, K., Mitchell, M., Bennett, A., Gurda, B.L., McKenna, R., Olson, N.H., Sinkovits, R.S., Potter, M., et al. (2012). Structural insight into the unique properties of adeno-associated virus serotype 9. J. Virol. *86*, 6947–6958. https://doi.org/10.1128/JVI.07232-11.

17. Cordier, L., Hack, A.A., Scott, M.O., Barton-Davis, E.R., Gao, G., Wilson, J.M., McNally, E.M., and Sweeney, H.L. (2000). Rescue of skeletal muscles of gamma-sarcoglycan-deficient mice with adeno-associated virus-mediated gene transfer. Mol. Ther. *1*, 119–129. https://doi.org/10.1006/mthe.1999.0019.

18. Herson, S., Hentati, F., Rigolet, A., Behin, A., Romero, N.B., Leturcq, F., Laforêt, P., Maisonobe, T., Amouri, R., Haddad, H., et al. (2012). A phase I trial of adeno-associated virus serotype 1-gamma-sarcoglycan gene therapy for limb girdle muscular dystrophy type 2C. Brain *135*, 483–492. https://doi.org/10.1093/brain/awr342.

19. Israeli, D., Cosette, J., Corre, G., Amor, F., Poupiot, J., Stockholm, D., Montus, M., Gjata, B., and Richard, I. (2019). An AAV-SGCG dose-response study in a gamma-sarcoglycanopathy mouse model in the context of mechanical stress. Mol. Ther. Methods Clin. Dev. *13*, 494–502. https://doi.org/10.1016/j.omtm.2019.04.007.

20. Buscara, L., Gross, D.A., and Daniele, N. (2020). Of rAAV and men: from genetic neuromuscular disorder efficacy and toxicity preclinical studies to clinical trials and back. J. Pers. Med. *10*, 258. https://doi.org/10.3390/jpm10040258.

21. Chicoine, L.G., Montgomery, C.L., Bremer, W.G., Shontz, K.M., Griffin, D.A., Heller, K.N., Lewis, S., Malik, V., Grose, W.E., Shilling, C.J., et al. (2014). Plasmapheresis eliminates the negative impact of AAV antibodies on microdystrophin gene expression following vascular delivery. Mol. Ther. *22*, 338–347. https://doi.org/10.1038/mt.2013.244.

22. Chicoine, L.G., Rodino-Klapac, L.R., Shao, G., Xu, R., Bremer, W.G., Camboni, M., Golden, B., Montgomery, C.L., Shontz, K., Heller, K.N., et al. (2014). Vascular delivery of rAAVrh74.MCK.GALGT2 to the gastrocnemius muscle of the rhesus macaque stimulates the expression of dystrophin and laminin alpha2 surrogates. Mol. Ther. *22*, 713–724. https://doi.org/10.1038/mt.2013.246.

23. Mendell, J.R., Chicoine, L.G., Al-Zaidy, S.A., Sahenk, Z., Lehman, K., Lowes, L., Miller, N., Alfano, L., Galliers, B., Lewis, S., et al. (2019). Gene delivery for limb-girdle muscular dystrophy type 2D by isolated limb infusion. Hum. Gene Ther. *30*, 794–801. https://doi.org/10.1089/hum.2019.006.

24. Zygmunt, D.A., Crowe, K.E., Flanigan, K.M., and Martin, P.T. (2017). Comparison of serum rAAV serotype-specific antibodies in patients with duchenne muscular dystrophy, becker muscular dystrophy, inclusion body myositis, or GNE myopathy. Hum. Gene Ther. *28*, 737–746. https://doi.org/10.1089/hum.2016.141.

25. Potter, R.A., Griffin, D.A., Sondergaard, P.C., Johnson, R.W., Pozsgai, E.R., Heller, K.N., Peterson, E.L., Lehtimäki, K.K., Windish, H.P., Mittal, P.J., et al. (2018). Systemic delivery of dysferlin overlap vectors provides long-term gene expression and functional improvement for dysferlinopathy. Hum. Gene Ther. *29*, 749–762. https://doi.org/10.1089/hum.2017.062.

26. Pozsgai, E.R., Griffin, D.A., Heller, K.N., Mendell, J.R., and Rodino-Klapac, L.R. (2016). beta-Sarcoglycan gene transfer decreases fibrosis and restores force in LGMD2E mice. Gene Ther. *23*, 57–66. https://doi.org/10.1038/gt.2015.80.

27. Griffin, D.A., Pozsgai, E.R., Heller, K.N., Potter, R.A., Peterson, E.L., and Rodino-Klapac, L.R. (2021). Preclinical systemic delivery of adeno-associated α-sarcoglycan gene transfer for limb-girdle muscular dystrophy. Hum. Gene Ther. *32*, 390–404. https://doi.org/10.1089/hum.2019.199.

28. Salva, M.Z., Himeda, C.L., Tai, P.W., Nishiuchi, E., Gregorevic, P., Allen, J.M., Finn, E.E., Nguyen, Q.G., Blankinship, M.J., Meuse, L., et al. (2007). Design of tissue-specific regulatory cassettes for high-level rAAV-mediated expression in skeletal and cardiac muscle. Mol. Ther. *15*, 320–329. https://doi.org/10.1038/sj.mt.6300027.

29. Ferrari, F.K., Samulski, T., Shenk, T., and Samulski, R.J. (1996). Second-strand synthesis is a rate-limiting step for efficient transduction by recombinant adeno-associated virus vectors. J. Virol. *70*, 3227–3234. https://doi.org/10.1128/jvi.70.5.3227-3234.1996.

30. Fisher, K.J., Gao, G.P., Weitzman, M.D., DeMatteo, R., Burda, J.F., and Wilson, J.M. (1996). Transduction with recombinant adeno-associated virus for gene therapy is limited by leading-strand synthesis. J. Virol. *70*, 520–532. https://doi.org/10.1128/jvi.70.1.520-532.1996.

31. McCarty, D.M., Monahan, P.E., and Samulski, R.J. (2001). Self-complementary recombinant adeno-associated virus (scAAV) vectors promote efficient transduction independently of DNA synthesis. Gene Ther. *8*, 1248–1254. https://doi.org/10.1038/sj.gt.3301514.

32. Angelini, C. (2020). LGMD. Identification, description and classification. Acta Myol. *39*, 207–217. https://doi.org/10.36185/2532-1900-024.

33. Rocha, C.T., and Hoffman, E.P. (2010). Limb-girdle and congenital muscular dystrophies: current diagnostics, management, and emerging technologies. Curr. Neurol. Neurosci. Rep. *10*, 267–276. https://doi.org/10.1007/s11910-010-0119-1.

34. Potter, R.A., Griffin, D.A., Heller, K.N., Peterson, E.L., Clark, E.K., Mendell, J.R., and Rodino-Klapac, L.R. (2021). Dose-escalation study of systemically delivered rAAVrh74.MHCK7.micro-dystrophin in the mdx mouse model of duchenne muscular dystrophy. Hum. Gene Ther. *32*, 375–389. https://doi.org/10.1089/hum.2019.255.

35. Zhu, X., Hadhazy, M., Groh, M.E., Wheeler, M.T., Wollmann, R., and McNally, E.M. (2001). Overexpression of gamma-sarcoglycan induces severe muscular dystrophy. Implications for the regulation of Sarcoglycan assembly. J. Biol. Chem. *276*, 21785–21790. https://doi.org/10.1074/jbc.M101877200.

36. Holt, K.H., Lim, L.E., Straub, V., Venzke, D.P., Duclos, F., Anderson, R.D., Davidson, B.L., and Campbell, K.P. (1998). Functional rescue of the sarcoglycan complex in the BIO 14.6 hamster using delta-sarcoglycan gene transfer. Mol. Cell *1*, 841–848. https://doi.org/10.1016/s1097-2765(00)80083-0.

37. Sandonà, D., and Betto, R. (2009). Sarcoglycanopathies: molecular pathogenesis and therapeutic prospects. Expert Rev. Mol. Med. *11*, e28. https://doi.org/10.1017/s1462399409001203.

38. Smith, L.R., and Barton, E.R. (2018). Regulation of fibrosis in muscular dystrophy. Matrix Biol. *68-69*, 602–615. https://doi.org/10.1016/j.matbio.2018.01.014.

39. Rodino-Klapac, L.R., Pozsgai, E.R., Lewis, S., Griffin, D.A., Meadows, A.S., Lehman, K.J., Church, K., Reash, N.F., Iammarino, M.A., Lowes, L.P., and Mendell, J.R. (2021). Safety, β-Sarcoglycan Expression, and Functional Outcomes from Systemic Gene Transfer of rAAVrh74.MHCK7.hSGCB in Limb-Girdle Muscular Dystrophy Type 2E/R4 (The 24th Annual Meeting of the American Society of Gene & Cell Therapy).

40. Rodino-Klapac, L.R., Janssen, P.M.L., Montgomery, C.L., Coley, B.D., Chicoine, L.G., Clark, K.R., and Mendell, J.R. (2007). A translational approach for limb vascular delivery of the micro-dystrophin gene without high volume or high pressure for treatment of Duchenne muscular dystrophy. J. Transl. Med. *5*, 45. https://doi.org/10.1186/1479-5876-5-45.

41. Sondergaard, P.C., Griffin, D.A., Pozsgai, E.R., Johnson, R.W., Grose, W.E., Heller, K.N., Shontz, K.M., Montgomery, C.L., Liu, J., Clark, K.R., et al. (2015). AAV.Dysferlin overlap vectors restore function in dysferlinopathy animal models. Ann. Clin. Transl. Neurol. *2*, 256–270. https://doi.org/10.1002/acn3.172.

42. Hakim, C.H., Wasala, N.B., and Duan, D. (2013). Evaluation of muscle function of the extensor digitorum longus muscle ex vivo and tibialis anterior muscle in situ in mice. J. Vis. Exp. https://doi.org/10.3791/50183.

43. Beastrom, N., Lu, H., Macke, A., Canan, B.D., Johnson, E.K., Penton, C.M., Kaspar, B.K., Rodino-Klapac, L.R., Zhou, L., Janssen, P.M.L., and Montanaro, F. (2011). mdx(^{5}cv) mice manifest more severe muscle dysfunction and diaphragm force deficits than do mdx Mice. Am. J. Pathol. *179*, 2464–2474. https://doi.org/10.1016/j.ajpath.2011.07.009.

44. Moorwood, C., Liu, M., Tian, Z., and Barton, E.R. (2013). Isometric and eccentric force generation assessment of skeletal muscles isolated from murine models of muscular dystrophies. J. Vis. Exp. e50036. https://doi.org/10.3791/50036.

45. Rafael-Fortney, J.A., Chimanji, N.S., Schill, K.E., Martin, C.D., Murray, J.D., Ganguly, R., Stangland, J.E., Tran, T., Xu, Y., Canan, B.D., et al. (2011). Early treatment with lisinopril and spironolactone preserves cardiac and skeletal muscle in Duchenne muscular dystrophy mice. Circulation *124*, 582–588. https://doi.org/10.1161/CIRCULATIONAHA.111.031716.

46. Kobayashi, Y.M., Rader, E.P., Crawford, R.W., Iyengar, N.K., Thedens, D.R., Faulkner, J.A., Parikh, S.V., Weiss, R.M., Chamberlain, J.S., Moore, S.A., and Campbell, K.P. (2008). Sarcolemma-localized nNOS is required to maintain activity after mild exercise. Nature *456*, 511–515. https://doi.org/10.1038/nature07414.

47. Võikar, V., Polus, A., Vasar, E., and Rauvala, H. (2005). Long-term individual housing in C57BL/6J and DBA/2 mice: assessment of behavioral consequences. Genes Brain Behav. *4*, 240–252. https://doi.org/10.1111/j.1601-183X.2004.00106.x.